CLM-P688

CLM-P688

UKAEA

Preprint

MEASUREMENT OF LONG WAVELENGTH TURBULENCE IN A TOKAMAK BY EXTREME FAR FORWARD SCATTERING

D. E. EVANS
E. J. DOYLE
D. FRIGIONE
M. von HELLERMANN
A. MURDOCH

CULHAM LABORATORY
Abingdon Oxfordshire

1983

CLM-P 688

MEASUREMENT OF LONG WAVELENGTH TURBULENCE IN A TOKAMAK BY EXTREME FAR FORWARD SCATTERING

D E Evans, E J Doyle[1], D Frigione[2],
M von Hellermann[3], and A Murdoch[4]

UKAEA Culham Laboratory

Abingdon, Oxfordshire OX14 3DB, England
(EURATOM/UKAEA Fusion Association)

ABSTRACT

Oscillations induced on the profile of a gaussian CW CO_2 laser beam by being transmitted through the TOSCA tokamak plasma are confined within envelopes whose shapes are correctly predicted by theory, permitting plasma fluctuation intensity and wavelength to be deduced as functions of frequency by a curve fitting procedure. The analysis shows spontaneous density fluctuations integrated across the TOSCA minor diameter to be mainly transverse to the magnetic field, with intensity maxima between 40 and 100 kHz and $\tilde{n}_e(\nu) \propto \nu^{-2}$ towards higher frequencies. At 200 kHz $\tilde{n}_e(\nu)/n_e$ is about 10^4 times thermal, and the total fluctuation level $\tilde{n}_e/n_e$ is a few percent. Coherent oscillations near 100 kHz, associated with rotating MHD structure, are occasionally observed. Wavelengths are found to lie between 1 and 6 cm, and correspond to $\kappa_\perp \rho_i$ in the range 0.2 to 2.0 , ρ_i being the ion gyroradius for the prevailing plasma conditions.

(Accepted for publication in Plasma Physics)

1 University College, Cork, Ireland

2 Assoc EURATOM CNEN Fusion, CNEN Frascati, Italy

3 University of Essen, Essen, German Fed Rep

4 University of Oxford, England

March 1983

1. INTRODUCTION

Naturally occurring density fluctuations in magnetically confined controlled fusion research plasmas are of interest for the light they throw on transport and energy dissipative processes, and they have been extensively studied, by collective scattering of micro waves (e.g. Mazzucato, 1978), 10 μm laser radiation (Slusher and Surko, 1980; Surko and Slusher, 1980; Pots, Coumans, and Schram, 1981; Meyer and Mahn, 1981; Fahrbach et al, 1981) and FIR lasers (Semet et al, 1980). The maximum accessible fluctuation wavelength has generally been determined through the Bragg relation by the need to choose the probing wavelength short enough to avoid gross refraction, and the scattering angle large enough to avoid stray light.

Small oscillations on the profile of a gaussian beam transmitted through a plasma can be identified with extreme forward collective scattered radiation spontaneously heterodyning with the undeviated beam (Evans, von Hellermann and Holzhauer 1982; Slusher and Surko 1980). Measurement of these oscillations offers a means of investigating electron density fluctuations at wavelengths so long they scatter within the divergence of the probing beam and might hitherto have been dismissed as unobservable. By adopting this technique the maximum accessible wavelength is determined only by the size of the gaussian beam waist in the plasma and the problem of stray light is entirely circumvented. Calculations suggest that very long wavelength turbulence, like trapped ion modes in plasmas such as JET, may be impossible to measure by any alternative method (Koechlin, 1981).

Simple apparatus has been assembled on the TOSCA tokamak to investigate long wavelength low frequency fluctuations by this technique.

2. RELEVANT THEORY

Theory (Evans, von Hellermann and Holzhauer, 1982) based on Fresnel diffraction leads to an expression for the intensity profile of a gaussian beam in the front focal plane of a lens situated a focal length beyond a beam waist in a plasma. The plasma contains a localized phase disturbance in the form of a monochromatic wave travelling transverse to the beam axis and crossing it a distance z from the waist, as shown in Figure 1, and the interaction between the radiation and the plasma wave is assumed to be in the Raman-Nath rather than the Bragg regime (Klein and Cook, 1967).

To first order in $\Delta\phi = r_e \lambda L \tilde{n}_e$, the instantaneous intensity pattern generated by the phase grating $\Delta\phi \sin(\kappa x - \Omega t)$ and measured through a narrow slit parallel to the y-direction will be

$$I(u) = \frac{I_o}{\sqrt{\pi}\, W_f} \left(e^{-u^2} + \Delta\phi\, e^{-(v/2)^2} \left[e^{-A_-^2} \cos(\zeta v A_- + \Omega t) - e^{-A_+^2} \cos(\zeta v A_+ + \Omega t) \right] \right) \qquad \ldots(1)$$

$$= I_{dc} + I_{ac}$$

where the variables and parameters used above are identified in the accompanying TABLE I .

The first term represents the unperturbed gaussian beam, while the second, proportional to $\Delta\phi$, consists of two gaussians centred at $u = \pm v/2$, oscillating at the frequency Ω of the wave, but out of phase with each other by an amount depending upon the fluctuation wavelength through v and the axial position of the plasma disturbance through ζ .

Because of its oscillatory character, the term I_{ac} can readily be distinguished from I_{dc} under experimental conditions, and the ratio of the two gives $\Delta\phi$ independent of any calibration, provided v and ζ are known. What one can actually measure is the envelope of I_{ac}, either with a multichannel array which conveys both intensity and phase information, or with a single detector used to construct the envelope profile over a sequence of plasma discharges, losing phase information in the process. From the envelope profile it is possible to deduce v and ζ by a process of curve fitting.

The envelope is given by the following expression:

$$I_{ac,e} = \Delta\phi\, e^{-v^2/2}\, e^{-u^2}\, [e^{2uv} + e^{-2uv} - 2\cos\zeta v^2]^{\frac{1}{2}} \qquad \ldots(2)$$

which is displayed for various values of v and ζ in Figure 2. In this figure, the diagrams on the right hand side are the same as those on the left rotated through 180°. The envelope functions can be seen to be symmetric about the probe beam axis (u = 0), and bifurcated into twin maxima for small values of ζ .

When the disturbance is located precisely at the beam waist, $\zeta = 0$, the two oscillating gaussians are in exact antiphase, and the envelope simplifies to

$$I_{ac,e}(\zeta=0) = \Delta\phi\, e^{-v^2/2}\, e^{-u^2}\, [e^{uv} - e^{-uv}] \,. \qquad \ldots(3)$$

In these circumstances, the amplitude and position of the maxima depend on v in the way shown in Figure 3 , their separation being $\Delta u = \sqrt{2}$ for $v < 1$, and $v/2$ for $v >> 1$.

In general, when $\zeta \neq 0$ and equation (2) prevails, the ratio of the envelope amplitude at its centre (u = 0) to its amplitude at the maxima is a sensitive measure of v when $v < 1$.

Finally, if the disturbance is exactly at the plasma beam waist but the profile is measured in a plane a known distance z_f from the front focal plane, the envelope is still given by equation (2) , but with ζ replaced by $\zeta_f = z_f/z_{rf}$, and v replaced by $V = (W_f/W_s)v$, where W_s is the beam width parameter in the slit plane, and z_{rf} is the Rayleigh zone calculated for the front focal plane beam waist (see Appendix A). Under these conditions the value of ζ_f is determined by the layout of the experiment, and so it is at once possible to deduce v and hence the plasma disturbance wavelength even when the latter is very long ($v<<1$). The three experimental arrangements discussed above are summarized in Figure 4 .

3. EXPERIMENTAL ASSEMBLY

TOSCA (McGuire et al 1979, Robinson and Wootton 1977) is a small tokamak with major radius 30 cm and plasma minor radius 8.5 cm , electron temperature $T_e \sim 100 - 400$ eV, ion temperature $T_i \leq 100$ eV, n_e from 10^{12} to 3×10^{13} cm^{-3} , and B_ϕ from 0.3 to 1.0 tesla.

The optical arrangement adopted is the third one in Figure 4, with the plasma at the beam waist and the slit plane remote from the front focal plane of the Fourier transforming mirror. In these experiments, accordingly, there has been no attempt to locate the disturbance within the plasma, but the wavelength was open to determination.

A 2-3 watt TEM_{oo} mode beam from an Edinburgh Instruments Ltd PL2 CW CO_2 laser is directed vertically across a minor torus diameter and focussed to a 0.24 cm beam waist near the toroidal axis, as shown in Figure 5 . Reflecting optics are used throughout, except for the vacuum vessel windows, which were AR-coated ZnSe wedges.

On emerging from the plasma, the laser beam travels 5 m to the Fourier transforming mirror (f = 5 m) which reconverges it and directs it towards a slit 88 cm beyond the mirror. The slit plane being 4.12 m from the front focal plane, the corresponding Rayleigh zone is 7.5 m , making $\zeta_f = 0.55$. Since the Rayleigh zone at the plasma beam waist exceeds 3 m , while the whole extent of the plasma is less than 17 cm , the plasma fluctuations are effectively localized at the beam waist. The conditions discussed in the last paragraph of §2 are accordingly met for fitting a function of the form of equation (2) to the observed envelopes of the time dependent part of the beam profile. As the only free parameters are V and $\Delta\phi$, the best fit gives a measure of the product of fluctuation intensity and interaction length $\tilde{n}_e(\nu)\, L$, and of the fluctuation wavelength Λ .

The fraction of the beam transmitted through the slit is finally focussed onto a 3 mm^2 Ge:Au photoconducting detector cooled to liquid nitrogen temperature. This is followed by a matched low noise amplifier whose output is filtered (20-500 kHz), digitized, and stored for subsequent numerical analysis. The filter removes the direct current part of the signal so that only the comparatively small time-dependent component reaches the digitizer. The direct current power level on the detector is maintained near

0.2 watt, monitored by an ammeter in the detector bias circuit. The time-independent laser beam gaussian profile in the slit plane is measured by chopping the laser beam and recording the direct output from the detector.

The detector noise level in the absence of plasma is consistent with the NEP expected for this detector operated at 10.6 μm wavelength.

Since the component of the turbulence being measured is that whose $\underline{\kappa}$ vector is perpendicular to the slit, the latter can be rotated so as to direct attention to the toroidal or alternatively to the transverse component.

4. RESULTS

Figure 6 shows the time dependent part, I_{ac}, of the signal from the detector viewing radiation through a narrow slit located to one side ($u \cong 0.7$) of the gaussian beam spot, and oriented so as to see predominantly transverse waves. The plasma lifetime was 0.5 ms . The frequency range was 20-500 kHz; formation and extinction of the plasma are clearly shown, and the signal-to-noise ratio is about 5 . The associated spectral density $I^2_{ac}(\nu)$ shows the decrease towards higher frequencies characterizing many of our tokamak plasma observations, and contrasts with the flat spectrum of noise also shown.

Time resolved spectra of TOSCA plasmas lasting about 3 ms show an early phase of about 1 ms with fluctuations behaving as described above. This initial phase is succeeded by a quiet middle period during which the fluctuation spectra in this frequency interval are almost flat, featureless and noiselike. During the final millisecond there is a tendency for coherent modes to develop around 100 kHz as shown in Figure 7 . Here, a peak protruding about 15 dB above the surrounding turbulence has become well defined near 120 kHz . This effect is so marked in the plasma whose record is shown in Figure 8 that it can be seen not only in the spectrum, but in the time dependent voltage trace as well.

The spectrum of the penultimate millisecond of this particular plasma's life already displayed multiple maxima but these died away or coalesced to be survived by the dominant oscillation at about 85 kHz, as shown here. Such coherent oscillations towards the end of the plasma lifetime are frequently associated with MHD activity in the form of rotating magnetic islands.

Confining our attention to reproducible plasmas, we have constructed the envelopes of oscillating term profiles from sequences of approximately 50 similar plasma discharges by measuring fluctuations at each of 12 slit positions across the probe beam diameter. The procedure, illustrated schematically in Figure 9, consisted of recording the fluctuations $[I_{ac}(t)]_u$ at each slit position u, computing corresponding frequency power spectra $[I^2_{ac,e}(\nu)]_u$, then using these to deduce fluctuation envelope profiles $[I_{ac,e}(u)]_\nu$ for narrow ($\sim$1 kHz) bandwidths at a succession of frequencies ν.

Contrary to our initial expectations, the frequency power spectra $[I^2_{ac,e}(\nu)]_u$ are not identical to each other within the statistics, but instead show a strong dependence upon the location u of the viewing slit relative to the probe beam centre. A set of such power spectra, measured during the first millisecond of 50 reproducible 3-4 ms plasmas, and selected to illustrate this slit position dependence, is displayed in Figure 10. We cannot say *a priori* which if any of these distributions is the true frequency power spectrum of plasma fluctuations. In fact, the true plasma fluctuation power spectrum can be determined only when theoretical curves have been fitted to the fluctuation envelope profiles $[I_{ac,e}(u)]_\nu$, thereby identifying the value of $\Delta\phi$ to be associated with each value of frequency ν.

The time independent probe beam profile I_{dc} at the slit plane was also recorded, both to obtain its width for scaling slit position in terms of the dimensionless variable $u_s \equiv x_s/W_s$, and to measure its intensity for computing $\Delta\phi$. Experimental points and the best fit gaussian curve through them for a typical I_{dc} profile having $W_s = 0.406$ cm are shown in Figure 11.

Examples of time dependent beam profile envelopes $[I_{ac,e}(u)]_\nu$ calculated from a complete set of frequency distributions for the 1st millisecond of the reproducible plasmas already referred to, are exhibited in Figure 12. Each experimental point is the average of 4-5 independent plasma measurements and the error bars are standard deviations on each set.

These profiles can be seen to display the expected symmetry about the beam centre with well defined maxima located in every case near $u_s = \pm 0.7$, implying wavelengths longer than $\sim$ 1.4 cm.

A maximum likelihood procedure has been followed to identify that member of the family of theoretical curves that best fits the experimental points in each case. The values obtained in this way for the shape parameter V , attached to each curve in the figure, range from 0.2 to 1.0 , implying fluctuation wavelengths from 6.4 cm to 1.4 cm, that is, wavenumbers in the transverse direction of $1.0\ cm^{-1} \leqq \kappa_\perp \leqq 4.6\ cm^{-1}$. It is perhaps worth remarking that a conventional scattering experiment set up to observe fluctuations at these wavenumbers with this laser would call for scattering angles around 0.02° .

A striking feature of these fluctuations is that the frequencies and their associated wavelengths appear to be approximately inversely proportional to each other. This is shown in Figure 13, where frequencies plotted against corresponding wavenumbers lie on a reasonably well defined straight line that passes through the origin and has slope $v \cong 2.5 \times 10^5\ cm\ s^{-1}$. The phase velocities measured at each point are shown plotted as a function of frequency in Figure 14 . The inset in Figure 13 shows in histogram form how the points constituting the curve in that diagram are distributed in wavelength.

For prevailing values of the TOSCA magnetic field (0.46 tesla) and ion temperature (50 eV) , the ion gyroradius $\rho_i \cong 0.22$ cm, so the product $\kappa_\perp \rho_i$ lay in the range 0.2 to 1.5 , as can be seen in Figure 13, and as observed in other tokamak plasmas e.g. Equipe TFR 1977.

A plot of the values of the fluctuation intensity interaction length product $\tilde{n}_e(\nu)\ L/n_e$ determined by the curve fitting process just described, versus corresponding frequencies is shown in Figure 15, and this is our best estimate of the spectrum of density fluctuations integrated across the plasma diameter. Low frequency filtering is used in making these measurements, but it is unlikely that the maximum near 40 kHz is an artifact. Towards higher frequencies fluctuation levels decrease according to a power law ν^{-2}, which bears out observations of Lee et al (1981) made on localized fluctuations in the UCLA Microtor plasma. Similar power law behaviour has been observed by Pots et al (1981) in their hollow cathode discharge.

As applied in the present experiment, our technique measures the product $\tilde{n}_e L$, but precludes the determination of $\tilde{n}_e$ and L separately. Accordingly, to obtain the fluctuation level $\tilde{n}_e$ alone requires an independent estimate of L . Clearly L is bounded by the plasma diameter on one hand, and presumably by the fluctuation wavelength on the other. It might indeed be reasonable to identify L with the breadth of the "transport region" outside the q = 1 surface in the 3-regime tokamak model. Either consideration suggests L is of the order of cm's . But as we cannot with confidence specify it more closely, we retain L as an independent parameter in the discussion of fluctuation levels that follows, with the understanding that it is probably of the order of a few cm's.

The total fluctuation level, calculated from the points on the frequency spectrum according to

$$\tilde{n}_e = \frac{1}{L} \sqrt{\{\Delta\nu \; \Sigma[\tilde{n}_e(\nu)L]^2\}}$$
$$= \frac{2.6 \times 10^{11}}{L} \; \text{cm}^{-3},$$

which, for the plasma density at this time of 3.9×10^{12} cm^{-3}, amounts to a relative fluctuation level

$$\tilde{n}_e / n_e = \frac{6.7 \times 10^{-2}}{L} \; ,$$

or almost 7% if the interaction length L ∿ 1 cm . The frequency dependent relative fluctuation level at, say, 100 kHz, is

$$\tilde{n}_e(\nu)/n_e\big|_{100\ \text{kHz}} = \frac{1.0 \times 10^{-4}}{L} \; \text{cm}^{-3}\ \text{Hz}^{-\frac{1}{2}} \; .$$

In Appendix B we show that the thermal level of fluctuations at this stage in the plasma's lifetime, taking T_i = 50 eV, T_e = 200 eV, and $n_e = 3.9 \times 10^{12}$ cm^{-3} , is

$$\tilde{n}_e(\nu)/n_e\big|_{\text{thermal}} \cong 5 \times 10^{-9} \text{cm}^{-3}\text{Hz}^{-\frac{1}{2}} \; .$$

Thus, assuming interaction length L ∿ 1 cm , fluctuations observed at 100 kHz are approximately 10^4 times thermal in this first millisecond.

All the foregoing results are for fluctuations whose $\underline{\kappa}$ vector is transverse to the toroidal direction. A search for a component parallel to the toroidal direction in this and in subsequent milliseconds produced very much weaker signals, implying, according to the theory of our technique, $\kappa_{\parallel}$ very much smaller than $\kappa_{\perp}$, and leading us to ascribe our observations to waves propagating at an angle not exceeding 10°-15° away from the transverse direction.

Analyses similar to that detailed above have been performed on fluctuations measured in subsequent millisecond intervals in these plasmas. By the third millisecond, little evidence of proportionality between ν and $\kappa_{\perp}$ remains. Instead, the wavelengths deduced from the beam profiles tend to cluster around a single value of wavelength, viz $\Lambda \sim 1$ cm, as shown in the histogram inset in the ν - $\kappa_{\perp}$ diagram presented in Figure 16 . A comparison of this histogram with the similar one for the first millisecond underlines the contrast in the character of the earlier and the later fluctuations. The product of frequency and wavelength now ranges between 0.5-2.9 x 10^5 cm s^{-1} , marginally lower than in the first millisecond, as shown in Figure 14 .

By the third millisecond, the toroidal magnetic field has fallen to about 0.4 tesla. There was no direct measure of ion temperature but if T_i remained near 50 eV, then $\kappa_{\perp}\rho_i$ lay in the range 0.7 to 2.0 .

The total fluctuation level in the third millisecond,

$$\frac{\tilde{n}}{n_e} = \frac{0.6 \times 10^{11}}{L} \quad cm^{-3} ,$$

is significantly smaller than previously, and the frequency distribution at this time, shown by the open points in Figure 15, appears to be a simple modification of that measured earlier. Indeed, the two distributions seem to merge at frequencies beyond about 200 kHz. But whereas the earlier goes through a maximum $\tilde{n}_e(\nu)\ L/n_e \cong 2.5 \times 10^{-4}\ Hz^{-\frac{1}{2}}$ near 40 kHz , the later one peaks around $4\text{-}5 \times 10^{-5}\ Hz^{-\frac{1}{2}}$ at about 100 kHz.

Parameters deduced for these plasmas are summarized in TABLE II.

5. DISCUSSION

The wavelength structure of the plasma fluctuations has been deduced in this investigation from laser probe beam profiles analysed in terms of a model that assumes only a single wavelength to be present. If the actual plasma disturbance is characterized by a band of wavelengths, then this analysis can at best identify the wavelength of the dominant fluctuation component, and this is the interpretation we believe ourselves justified in placing upon our results.

That the beam profile analysis really measures a feature of the plasma disturbance and not simply something artificially induced by the experimental technique is evidenced by the contrasting wavelength distributions obtained for the two time intervals studied.

At both times, plasma fluctuations were found to be approximately transverse to the toroidal direction, and though it is not impossible that they were actually radial, it seems more reasonable to assume that we are dealing with poloidally directed fluctuations.

The phase velocities $\nu \cdot \Lambda$ were all found to lie between 0.5 and 5.0×10^5 cm s^{-1}. Assuming TOSCA's density profile is well represented by $n_e = n_{eo}(1-r^2/a^2)$ and its electron temperature profile by $T_e = T_{eo} \exp -(r/0.5a)^2$ with $T_{eo} = 250$ eV, and taking $B \sim 0.5$ tesla, the range of electron magnetic drift velocity v_{de} distributed across the plasma radius, shown in Figure 17, is found to coincide almost exactly with the velocities measured. We have been unable to determine from our measurements whether the fluctuation velocity is in the electron or the ion drift direction, nor can we comment on the possible bulk rotation of the plasma.

Provided phase between density and electric field fluctuations is correct, the diffusion coefficient associated with enhanced density fluctuations, modified to take into account that we measure the fluctuation interaction length product $\tilde{n}_e L$ rather than $\tilde{n}_e$ alone, is

$$D_\perp = \Delta\omega \, (L_{n_e}/L)^2 \, \left(\frac{\tilde{n}_e \, L}{n_e} \right)^2$$

where $L_{n_e} \equiv \left[\frac{1}{n_e} \frac{d n_e}{dr} \right]^{-1}$ is the density gradient scale length and $\Delta\omega$ is the angular frequency spectrum bandwidth. When the latter is not measured, it is sometimes arbitrarily set equal to the drift wave frequency, viz $\Delta\omega = \omega_{\star e}$ (see for e.g. Okabayashi and Arunasalam 1977). For the first millisecond we have adopted this

expedient and taken the representative frequency to be 40 kHz. On the other hand, the fluctuations during the third millisecond are characterized by a single wavelength having a spectrum of frequencies with a width $\sim$ 100 kHz, which we accordingly use to calculate $D_\perp$ in this case. Assuming an interaction length $L \sim 1$ cm, and the radius at which the transport is maximum to be 5 cm, giving $^{L}n_e \sim 4.7$ cm, leads to $D_\perp \sim 2 \times 10^4$ cm^2 s^{-1}, and $D_\perp \sim 0.5 \times 10^4$ cm^2 s^{-1} for the first and third milliseconds respectively.

At this radius, these correspond to particle confinement times $\tau = 3/16 \; r^2/D_\perp \sim 0.2$ ms and 1.0 ms, which are consistent with lifetimes obtained from independent diagnostics (e.g. McGuire 1979).

Time dependent profiles exhibiting asymmetry with respect to the intensities in the two wings are sometimes measured for both toroidal and transverse fluctuation components, and the suspicion that they are artifacts of the measurement is dispelled by the observation that the asymmetry can be controlled by varying the plasma conditions. An example is shown in Figure 18, which also shows smaller peak spacing than theory predicts. These observations might be accounted for by a small departure of the scattering conditions from pure Raman-Nath towards the Bragg regime. In any case, we find a correlation with the position of the plasma magnetic axis relative to the probe beam, skewness of the two being associated with asymmetry.

6. CONCLUSIONS

Oscillations induced on the profile of a gaussian laser beam by transmission across the vertical minor diameter of the TOSCA tokamak have been exploited to measure long wavelength plasma density fluctuations. Envelopes of the time dependent profiles have shapes predicted by the theory, and a curve fitting procedure accordingly determines wavelength and fluctuation intensity as a function of frequency.

In the 20-500 kHz interval under investigation plasma fluctuation energy is concentrated towards low frequencies, in contrast to noise, which is uniform over the band. Coherent oscillations near 100 kHz associated with rotating MHD structure are sometimes observed at the termination of the plasma.

Detailed analysis has been performed on beam profile envelopes constructed piecemeal from 50 reproducible plasma discharges that had a lifetime of 4 ms. Investigation was confined to the transverse component of the plasma fluctuation, as the toroidal component was negligibly small by comparison.

During the initial millisecond, wavenumbers ranging from 1 cm^{-1} to 7 cm^{-1} (wavelengths from 1 cm to 6 cm) in rough proportionality to the frequency, were revealed. They correspond to $0.2 \leq \kappa_\perp \rho_i \leq 1.5$ for the prevailing plasma conditions, and phase velocities were a few times 10^5 cm s^{-1}. The frequency spectrum of fluctuations passed through a maximum at 40 kHz and fell away as ν^{-2} towards higher frequencies. The total relative fluctuation level during the first millisecond was $\tilde{n}_e L/n_e \sim 6.7 \times 10^{-2}$ cm , and the frequency dependent fluctuation level at 100 kHz was of the order 10^4 times thermal.

Unlike the fluctuations observed in the first millisecond, those measured during the third millisecond had values of wavelength that clustered closely around a single value, namely $\Lambda \sim 1$ cm . These contrasting wavelength distributions encourage us to believe that our beam profile analysis actually measures a feature of the plasma disturbance and not some artifact of the experimental technique.

These third millisecond fluctuations have phase velocities of a few times 10^5 cm s^{-1} and $\kappa_\perp \rho_i$ for them lies between 1 and 2 if T_i = 50 eV. The frequency spectrum of these later fluctuations is flatter than for the earlier ones, and it passes through a

maximum near 100 kHz, at a value of $\tilde{n}_e(\nu)L/n_e$ between 4 and 5 times 10^{-5} cm $Hz^{-\frac{1}{2}}$. At high frequencies, it appears to merge with the ν^{-2} curve measured at the earlier time. The total fluctuation level during the third millisecond is $\tilde{n}_e L/n_e = 1.8 \times 10^{-2}$ cm. The enhanced density fluctuation diffusion coefficient turns out to have values $D_\perp \leqslant 10^4$ cm^2 s^{-1} which at a radius of a few cm corresponds to a particle confinement time of about 1 ms .

Asymmetric profiles associated with the skewness of the probe beam relative to the plasma magnetic axis were observed, but their significance is not as yet understood.

ACKNOWLEDGEMENT

EJD is supported by an Irish Department of Education maintenance grant, DF and MvH by EURATOM fellowships, and AM by a UK SERC award. All are grateful for the hospitality of the Culham Laboratory.

APPENDIX A

In this appendix we derive the time-dependent beam profile for the case where the plasma lies at a gaussian beam waist and the slit is remote from the focal plane, as diagrammed in Fig A1 .

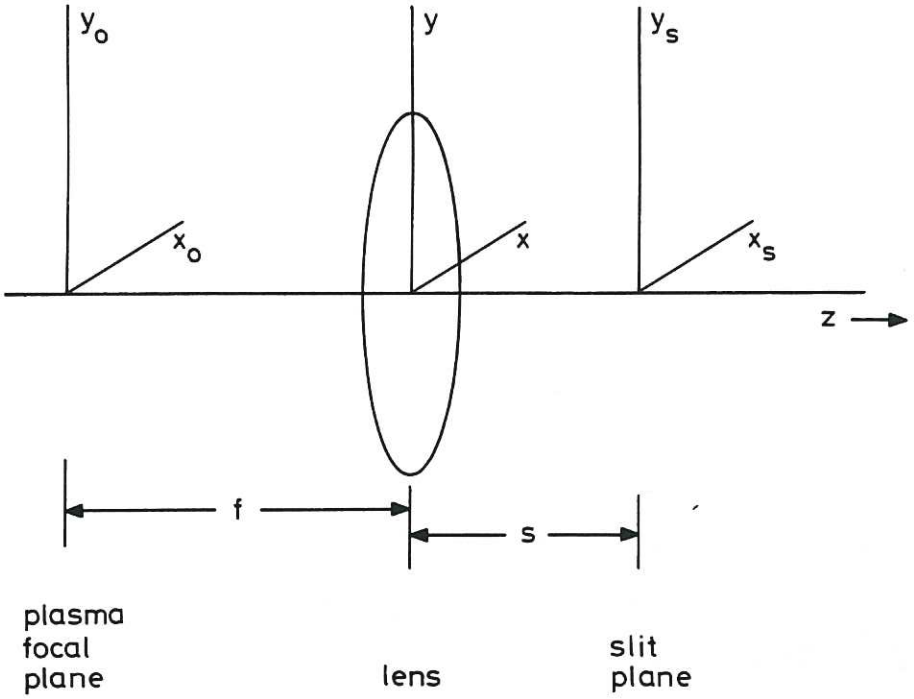

We use the basic theorems of Fourier optics (Goodman,1968) namely, the optical amplitudes U_1 and U_2 in two parallel planes separated by a distance z are related by a convolution with the Fresnel kernel h_z , viz

$$U_2 = h_z * U_1 \quad , \qquad \ldots(A1)$$

and, the amplitudes U_o and U_f in the pair of focal planes on either side of a simple lens are a fourier transform pair:

$$U_f = \tilde{U}_o \ . \qquad \ldots(A2)$$

According to these theorems, amplitudes U_s and U_o are related by

$$U_s = h_z * U_f = h_z * \tilde{U}_o \ . \qquad \ldots(A3)$$

Amplitude U_o is a gaussian beam waist modified by a phase factor representing a sinusoidal plasma wave, amplitude $\Delta\varphi$, travelling in the x-direction transverse to the optical axis.

That is $U_o = U_g\, t$

where $t = e^{i\,\Delta\varphi\,\sin(Kx-\Omega t)}$

$$\approx 1 + \tfrac{1}{2}\,\Delta\varphi\,\left[\, e^{i\,(Kx-\Omega t)} - e^{-i\,(Kx-\Omega t)} \,\right] . \qquad \ldots(A4)$$

Then $\tilde{U}_o = \widetilde{U_g t} = \tilde{U}_g * \tilde{t}$ by the convolution theorem. Substituting this into (A3) and making use of the commutative property of convolutions results in

$$U_s = h_z * [\, \tilde{U}_g * \tilde{t}\,] = \tilde{t} * [\, h_z * \tilde{U}_g\,] . \qquad \ldots(A5)$$

Since U_g is a gaussian beam waist amplitude distribution at one focal plane, $\tilde{U}_g$ is the conjugate gaussian beam waist at the other, and $h_z * \tilde{U}_g$ is accordingly a gaussian beam a distance z from the beam waist. This is well known and can be written down without calculation (Siegman, 1971) as

$$h_z * \tilde{U}_g \equiv U_{gs} = \frac{1}{\sqrt{\pi}\, W_s}\; e^{-\frac{1}{2}(1+i\zeta_f)(x_s^2/W_s^2)} . \qquad \ldots(A6)$$

We have next to calculate $\tilde{t}$ using (A4):

$$\tilde{t} = \int_{-\infty}^{+\infty} e^{-i\,2\pi\,\nu x}\, t(x)\, dx \quad \text{with} \quad \nu \equiv \frac{x}{\lambda\, f}$$

$$\tilde{t} = \delta(\nu) + \tfrac{1}{2}\,\Delta\varphi\,\left[\, e^{-i\Omega t}\,\delta(\tfrac{K}{2\pi} - \nu) - e^{+i\Omega t}\,\delta(\tfrac{K}{2\pi} + \nu)\,\right] \qquad \ldots(A7)$$

and construct its convolution with U_{gs}, the latter given by (A6). The outcome is proportional to

$$e^{-\frac{1}{2}(1+i\zeta_f)u_s^2} + \tfrac{1}{2}\,\Delta\varphi\,\left[\, e^{-i\Omega t}\, e^{-\frac{1}{2}(1+i\zeta_f)(\frac{K}{2\pi} - \frac{x_s}{\lambda f})^2} - e^{+i\Omega t}\, e^{-\frac{1}{2}(1+i\zeta_f)(\frac{K}{2\pi} + \frac{x_s}{\lambda f})^2}\,\right] .$$

Using the dimensionless quantities $u_s \equiv x_s/W_s$ and $V \equiv (W_f/W_s)\, KW_o \equiv (W_f/W_s)\, v$, the foregoing expression becomes

$$U_s = \frac{1}{\sqrt{\pi}\, W_s} \left\{ e^{-\frac{1}{2}(1+i\zeta_f)u_s^2} + \tfrac{1}{2}\,\Delta\varphi \left[e^{-i\Omega t}\, e^{-\frac{1}{2}(1+i\zeta_f)(u_s-V)^2} - e^{+i\Omega t}\, e^{-\frac{1}{2}(1+i\zeta_f)(u_s+V)^2} \right] \right\} . \qquad \ldots(A8)$$

Finally, we calculate the intensity by multiplying U_s by its complex conjugate U_s^* . Integration of the intensity along the y-direction is tacitly understood. Then

$$U_s U_s^* = \frac{1}{\sqrt{\pi}\, W_s} \left\{ e^{-u_s^2} + \Delta\varphi\, e^{-V^2/4} \left[e^{-A_-^2} \cos(\Omega t - \zeta_f V A_-) - e^{-A_+^2} \cos(\Omega t - \zeta_f V A_+) \right] \right\} \qquad \ldots(A9)$$

$$= I_{dc} + I_{ac} .$$

To construct the envelope of the time-dependent term we rewrite I_{ac} as

$$I_{ac} = \frac{1}{\sqrt{\pi}\, W_s}\, \Delta\varphi\, e^{-V^2/4} \left[g \cos \Omega t + h \sin \Omega t \right]$$

and form $I_{ac,e} = \dfrac{1}{\sqrt{\pi}\, W_s}\, \Delta\varphi\, e^{-V^2/4} \sqrt{(g^2 + h^2)}$,

that is

$$I_{ac,e} = \frac{1}{\sqrt{\pi}\, W_s}\, \Delta\varphi\, e^{-V^2/2}\, e^{-u_s^2} \left[e^{-2u_s V} + e^{+2u_s V} - 2 \cos \zeta_f V^2 \right]^{\frac{1}{2}} \qquad \ldots(A10)$$

and the relative phase, as a function of u_s across the profile, is given by Φ, where

$$\tan \Phi = \frac{e^{-A_-^2} \cos \zeta_f VA_- - e^{-A_+^2} \cos \zeta_f VA_+}{e^{-A_+^2} \sin \zeta_f VA_+ - e^{-A_-^2} \sin \zeta_f VA_-} \quad . \qquad \ldots(A11)$$

APPENDIX B

Thermal Density Fluctuation Level

We calculate $\tilde{n}_e(\omega=0)/n_e$ using the relation between the frequency spectrum of density fluctuations $\tilde{n}_e(\omega)$ and the scattering form factor $S(\underline{k},\omega)$ [Pots et al,1981]:

$$\tilde{n}_e(\omega)/n_e = \left[\frac{1}{n_e(2\pi)^3} \int S(\underline{k},\omega) d^3k \right]^{\frac{1}{2}}$$

$$= \left[\frac{1}{n_e(2\pi)^3} \int S(k,\omega)\ 4\pi k^2\ dk \right]^{\frac{1}{2}} . \qquad \ldots(B1)$$

The general expression for the form factor for a thermal plasma is [Evans and Katzenstein,1969]

$$S(k,\omega) = \frac{\left| k^2\lambda_D^2 + Z\ W(x) \right|^2\ a_e\ e^{-a_e^2x^2} + Z\left|W(a_ex)\right|^2\ e^{-x^2}}{\sqrt{\pi}\ kv_i\ \left| k^2\lambda_D^2 + W(a_ex) + Z(T_e/T_i)\ W(x) \right|^2} \qquad \ldots(B2)$$

where $x \equiv \frac{\omega}{kv_i}$ $\quad a_e \equiv \sqrt{(m_e/M)}\ \sqrt{(T_i/T_e)}$ and $W(x)$ is the plasma dispersion function. Other symbols have their usual meanings. Setting $\omega=0$ and writing ion thermal velocity $v_i = \sqrt{2}\ \omega_{pi}\lambda_D[Z(T_e/T_i)]^{-\frac{1}{2}}$, ω_{pi} being the (circular) ion plasma frequency, we have

$$S(k,\omega=0) = \frac{\sqrt{(ZT_e/T_i)}}{\sqrt{(2\pi)}\ \omega_{pi}\ k\lambda_D} \quad \frac{Z + a_e[k^2\lambda_D^2 + Z(T_e/T_i)]^2}{[1 + k^2\lambda_D^2 + Z(T_e/T_i)]^2} \qquad \ldots(B3)$$

and

$$\left[\frac{\tilde{n}_e(\omega=0)}{n_e}\right]^2 = \frac{\sqrt{(ZT_e/T_i)}}{[\sqrt{(2\pi)}]^5 n_e\ \lambda_D^3\ \omega_{pi}} \int_0^1 \frac{Z+a_e[k^2\lambda_D^2 + Z(T_e/T_i)]^2}{[1 + k^2\lambda_D^2 + Z(T_e/T_i)]^2} d(k^2\lambda_D^2)$$

$$\ldots(B4)$$

restricting integration to the collective regime by integrating between the limits $0 < k^2\lambda_D^2 < 1$.

The result is

$$\left[\frac{\tilde{n}_e(\omega=0)}{n_e}\right]^2 = \frac{\sqrt{(ZT_e/T_i)}}{[\sqrt{(2\pi)}]^5\,\omega_{pi}\,(n_e\lambda_D^3)}\left\{\frac{Z}{[1+Z(T_e/T_i)][2+Z(T_e/T_i)]}\right.$$

$$\left. + a_e\left[1 + \frac{Z}{[1+Z(T_e/T_i)][2+Z(T_e/T_i)]} - 2\,\ell n\,\frac{[2+Z(T_e/T_i)]}{[1+Z(T_e/T_i)]}\right]\right\} \qquad \ldots(B5)$$

If $T_e/T_i \gg 1$ $\quad \left[\frac{\tilde{n}_e(\omega=0)}{n_e}\right]^2 \rightarrow \frac{\sqrt{Z}\,\sqrt{(m_e/M)}}{[\sqrt{(2\pi)}]^5\;\omega_{pi}\;(n_e\lambda_D^3)}$

$T_e/T_i \ll 1$ $\quad \left[\frac{\tilde{n}_e(\omega=0)}{n_e}\right]^2 \rightarrow \frac{[1+\frac{1}{2}-\ell n\ 4]\,\sqrt{Z}\,\sqrt{(m_e/M)}}{[\sqrt{(2\pi)}]^5\;\omega_{pi}\;(n_e\lambda_D^3)}$

and the maximum occurs for $T_e/T_i \approx 0.5$, when

$$\left[\frac{\tilde{n}_e(\omega=0)}{n_e}\right]^2 = \frac{0.19\,\sqrt{Z}}{[\sqrt{(2\pi)}]^5\;\omega_{pi}\;(n_e\lambda_D^3)} \quad .$$

T A B L E I

Symbols used in the text.

a	tokamak limiter radius
$A_{\pm}$	$\equiv u \pm v/2$ or $u_s \pm v_s/2$
B	magnetic field
B_{ϕ}	magnetic field in the toroidal direction
$D_{\perp}$	perpendicular diffusion coefficient
I_o	intensity of incident laser beam at its centre
$I(u)$	laser beam intensity profile
I_{dc}	time-independent intensity component
I_{ac}	time-dependent intensity component
$I_{ac,e}$	envelope of I_{ac}
$I^2_{ac}(\nu)$	spectral density associated with I_{ac}
$[I_{ac}(t)]_u$	time-dependent intensity measured at slit position u .
$[I^2_{ac}(\nu)]_u$	spectral power density associated with $[I_{ac}(t)]_u$
$[I_{ac,e}(u)]_\nu$	envelope of fluctuating beam profile for frequency ν .
L	interaction length
L_{n_e}	density gradient scale length $L^{-1}_{n_e} \equiv \frac{1}{n_e}\frac{d}{dr}\frac{n_e}{}$
n_e	electron density (cm^{-3})
n_{eo}	spatial profile peak electron density
$\tilde{n}_e$	electron density fluctuation (cm^{-3})
$\tilde{n}_e(\nu)$	frequency dependent electron density fluctuation (cm^{-3} $Hz^{-\frac{1}{2}}$)
q	tokamak safety factor
r	radius
r_e	classical electron radius
t	time

TABLE I (continued)

T_e	electron temperature
T_{eo}	radial profile peak T_e
T_i	ion temperature
u	$\equiv x_f/W_f$, position relative to, and transverse to laser beam axis, normalized to width of gaussian beam, especially in front focal plane.
u_s	$\equiv x_s/W_s$
v	$\equiv \kappa W_o$ wavelength parameter
V	$\equiv (W_f/W_s)v$ modified wavelength parameter; used when slit is remote from front focal plane.
v_{de}	electron drift velocity
W	gaussian beam width parameter, defined so: $I = \frac{I_o}{\sqrt{\pi}\, W} e^{-x^2/W^2}$
W_o	gaussian beam waist parameter, usually on plasma side of lens.
W_f	gaussian beam waist parameter in lens front focal plane
W_s	gaussian beam width parameter in slit plane
x	position relative to and transverse to laser beam axis
x_f	x at front focal plane
x_s	x at slit plane
z	axial position relative to beam waist W_o
z_f	axial position relative to beam waist W_f
z_r	$\equiv \frac{2\pi W_o^2}{\lambda}$ Rayleigh zone corresponding to plasma side focal plane
z_{rf}	$\equiv \frac{2\pi W_f^2}{\lambda}$ Rayleigh zone corresponding to front focal plane
ζ	$\equiv z/z_r$ axial position normalized to Rayleigh zone, on plasma side
ζ_f	$\equiv z_f/z_{rf}$ axial position normalized to Rayleigh zone on front focal plane side
$\underline{\kappa}$	fluctuation wave vector

TABLE I (continued)

$\kappa_{\parallel}$ $\kappa_{\perp}$	components of fluctuation wavevector parallel and perpendicular to magnetic field
λ	laser wavelength
Λ	fluctuation wavelength
ν	fluctuation frequency
ρ_i	ion gyroradius
$\Delta\phi$	phase shift; for plasma-induced phase shift, $\Delta\phi = r_e \lambda L \tilde{n}_e$
$\omega_{\star e}$	electron drift wave frequency
Ω	fluctuation angular frequency

T A B L E II

	1st ms	3rd ms
B_ϕ (tesla)	0.46	0.39
n_{eo} (cm^{-3})	3.9×10^{12}	3.3×10^{12}
$\tilde{n}_e L$ (cm^{-3})	2.6×10^{11}	0.6×10^{11}
T_i (eV)	50	50 (20?)
T_{eo} (eV)	250	250
ρ_i (cm)	0.22	0.26 (0.17)
V	0.2 - 1.5	0.6 - 1.7
Λ (cm)	6.4 - 0.9	2.2 - 0.8
$\kappa_\perp$ (cm^{-1})	1.0 - 7.0	2.9 - 7.9
$\Lambda \cdot \nu$ ($cm\ s^{-1}$)	$1 - 5 \times 10^5$	$0.5 - 3 \times 10^5$
$\tilde{n}_e L / n_e$ (cm)	6.7×10^{-2}	1.8×10^{-2}
$D_\perp$ ($cm^2\ s^{-1}$) (for L=1 cm)	2.4×10^4	0.5×10^4
τ (ms) (for a=5 cm)	0.2	1.0

REFERENCES

Equipe TFR (1977) Proceedings 8th European Conference on Controlled Nuclear Fusion and Plasma Physics Prague

Equipe TFR (1980) VIIIth International Conference on Plasma Physics and Controlled Nuclear Fusion Research Brussels IAEA-CN-38/N-5

Evans D E and Katzenstein J (1969) Reports on Progress in Physics 32 207-271

Evans D E, von Hellermann M, and Holzhauer E (1982) Plasma Physics 24 819-834

Fahrbach H U, Koppendorfer W, Munich M, Neuhauser J, Rohr H, Schram G, Sommer J, and Holzhauer E (1981) Nuclear Fusion 21 257

Goodman J W (1968) Introduction to Fourier Optics pub. McGraw-Hill Inc

Klein W R and Cook,Bill D (1967) IEEE Transactions on Sonics and Ultrasonics SU-14 123-134

Koechlin F (1981) Private communication

Lee P, Luhmann Jr N C, Park H, Peebles W A, Taylor R J, and Yu C X (1981) Report PPG556 UCLA Centre for Plasma Physics

Mazzucato E (1978) Physics of Fluids 21 1063

McGuire K M, Robinson D C, Wootton A J (1979) Proceedings 10th European Conference on Plasma Physics and Controlled Fusion Research IAEA Vienna 1 424

McGuire K M (1979) D Phil thesis, Univ of Oxford

Meyer J and Mahn C (1981) Phys Rev Letters 46 1206

Okabayashi M and Arunasalam V (1977) Nuclear Fusion 17 497-513

Pots B F M, Coumans J J H, and Schram D C (1981) Physics of Fluids 24 517

Robinson D C and Wootton A J (1977) Proceedings 8th European Conference on Controlled Fusion and Plasma Physics Prague 1 21

Semet A, Mase A, Peebles W A, Luhmann Jr N C, and Zweben S (1980) Phys Rev Letters 45 445

Siegman A E (1971) An Introduction to Lasers and Masers pub McGraw-Hill Inc

Slusher R E and Surko C M (1980) Physics of Fluids 23 472

Surko C M and Slusher R E (1980) Physics of Fluids 23 2425

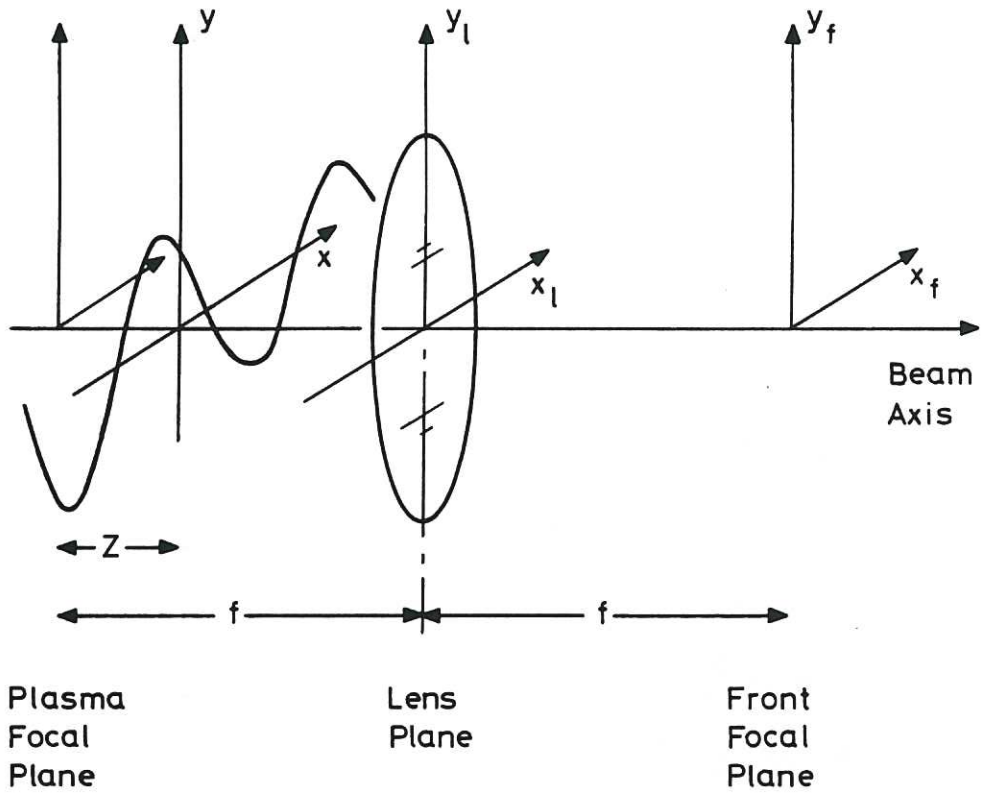

Fig.1 Configuration of plasma disturbance, lens, and viewing plane for which the probe beam profile is calculated.

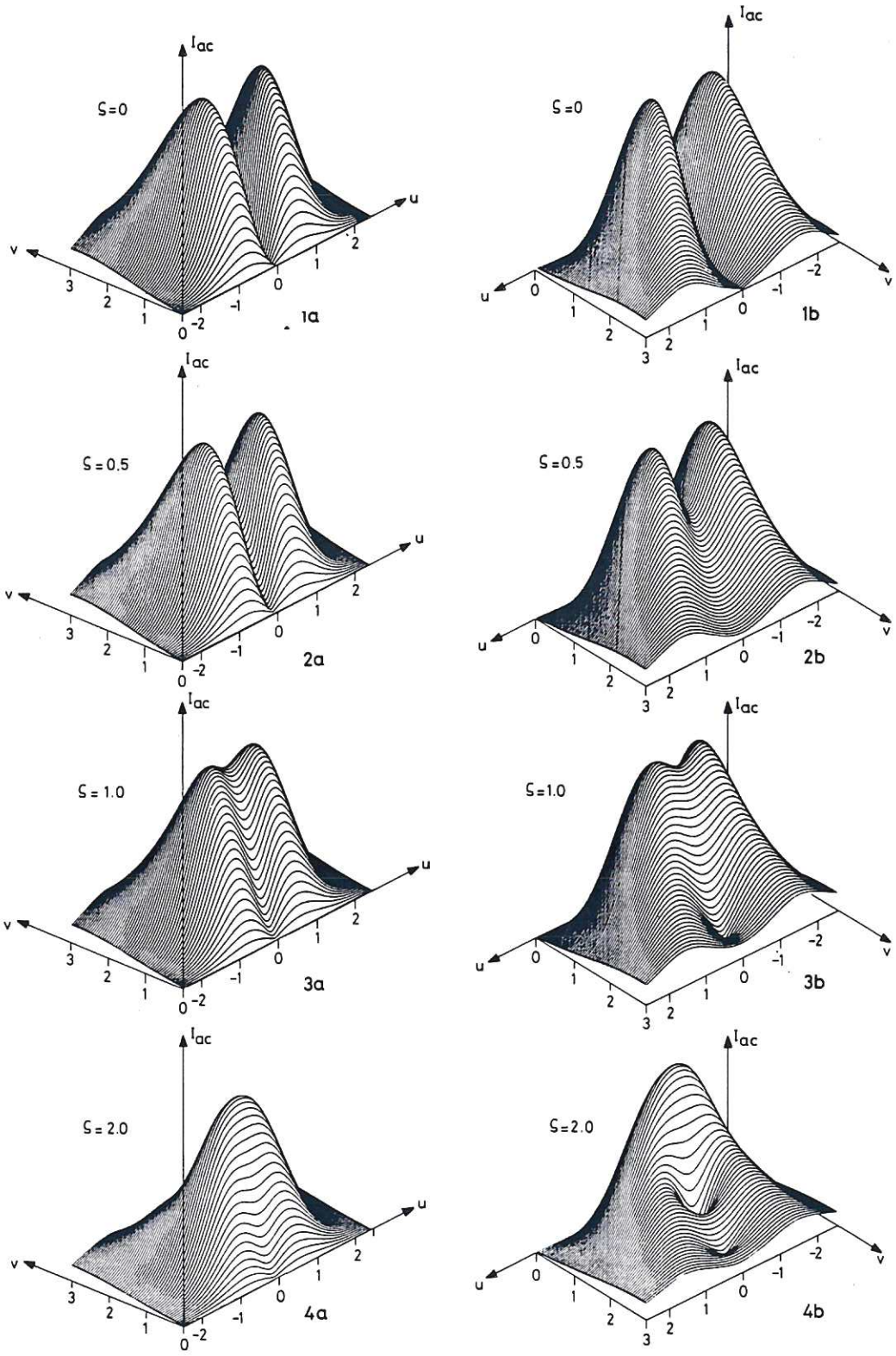

Fig.2 Variation of the envelope of the time dependent part of the beam profile produced by changes in the wavelength (through $v \equiv \kappa W_0 \equiv 2\pi W_0/\Lambda$), and in location (through $\zeta \equiv z/z_T$) of the plasma disturbance.

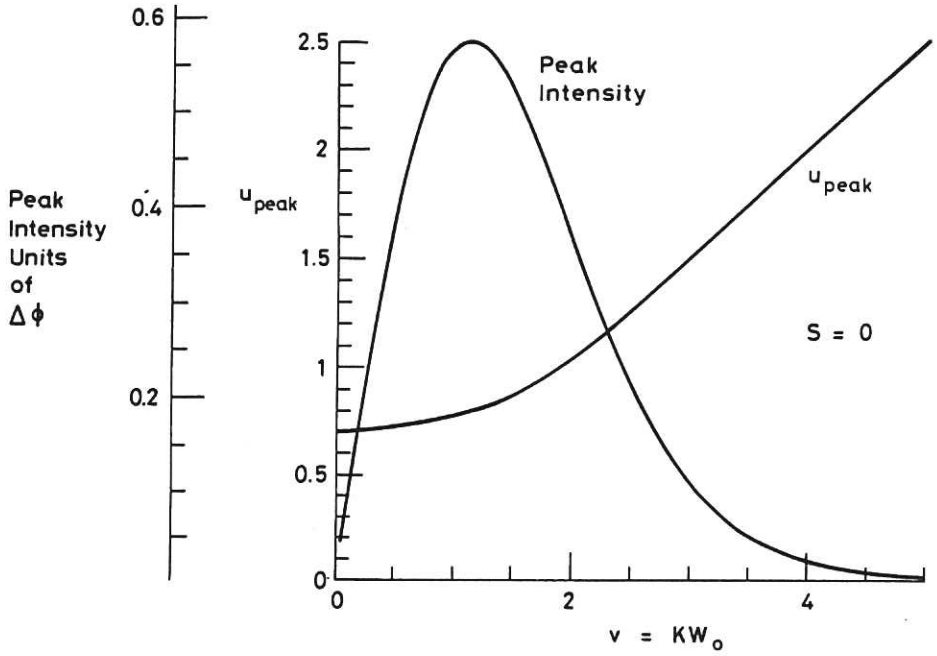

Fig.3 Dependence of peak height and separation (= $2u_{peak}$) on the fluctuation wavelength, through the parameter v. Focal plane to focal plane case ($\zeta = 0$) is illustrated.

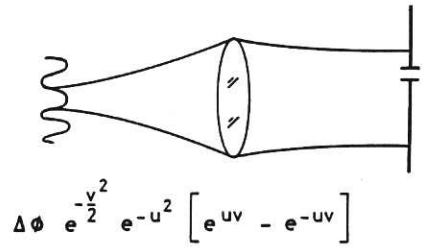

$$\Delta\phi\ e^{-\frac{v^2}{2}}\ e^{-u^2}\left[e^{uv} - e^{-uv}\right]$$

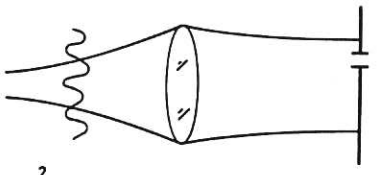

$$\Delta\phi\ e^{-\frac{v^2}{2}}\ e^{-u^2}\left[e^{2uv} + e^{-2uv} - 2\cos\zeta v^2\right]^{1/2}$$

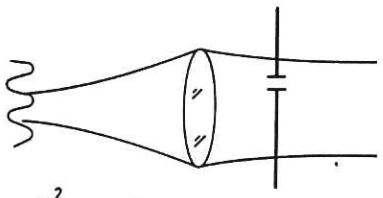

$$\Delta\phi\ e^{-\frac{V^2}{2}}\ e^{-u^2}\left[e^{2uV} + e^{-2uV} - 2\cos\zeta v^2\right]^{1/2}$$

$$V \equiv \frac{W_f}{W_s}\ v$$

Fig.4 Envelope functions for various configurations of the plasma disturbance, the lens, and the slit plane. The last is the one adopted for the experiment described here.

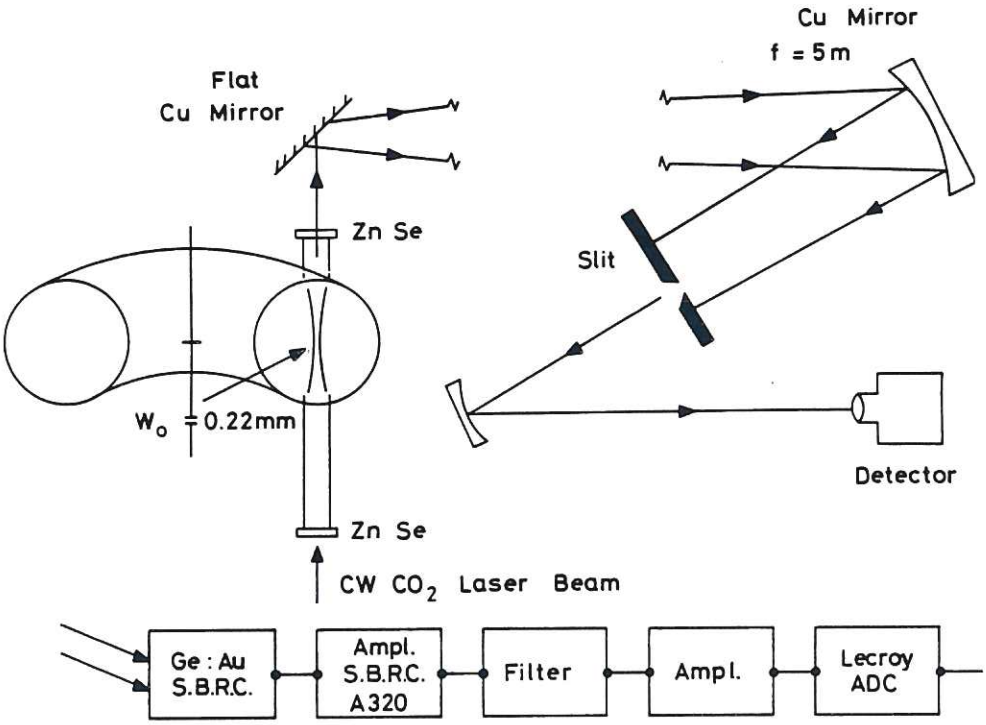

Fig.5 Schematic of the experimental layout on the TOSCA torus.

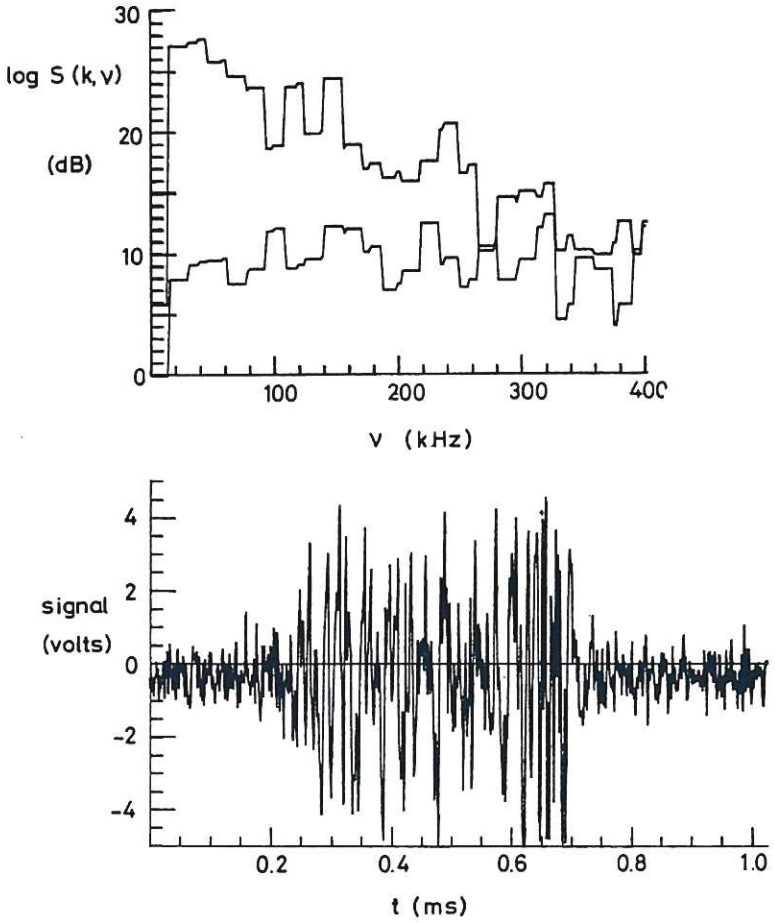

Fig.6 Lower part shows time-dependent signal I_{ac} over a 1 ms interval. Plasma was present from 0.25 ms to 0.70 ms. Upper part contrasts flat power spectrum of noise with approximate ν^{-2} spectrum of plasma fluctuations.

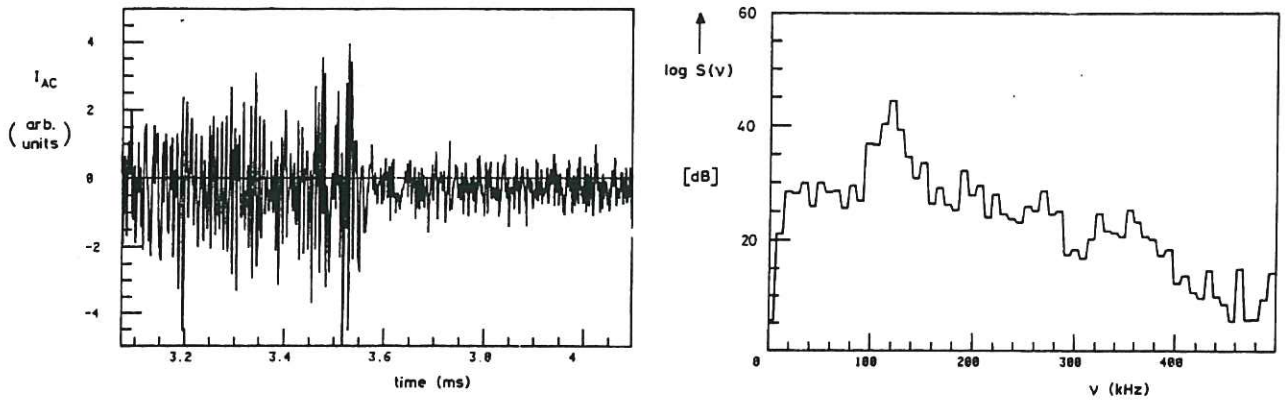

Fig.7 Record of density fluctuations during the last 0.5 ms of a 3 ms plasma, with associated frequency spectrum on a log-linear scale, showing the peak at 120kHz.

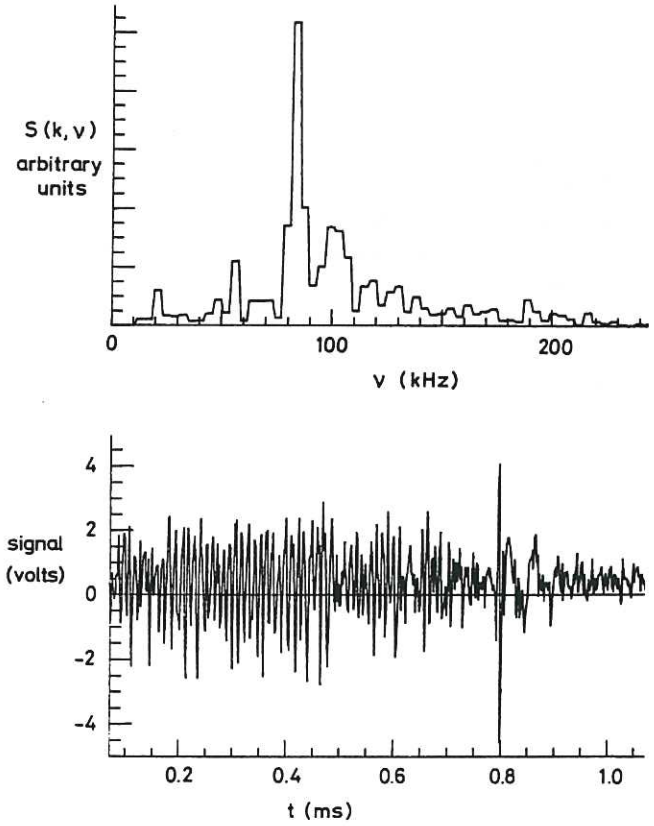

Fig.8 Development of coherent modes at the end of the plasma lifetime apparent not only in the (linear-linear) frequency spectrum, but even in the time-dependent signal I_{ac}.

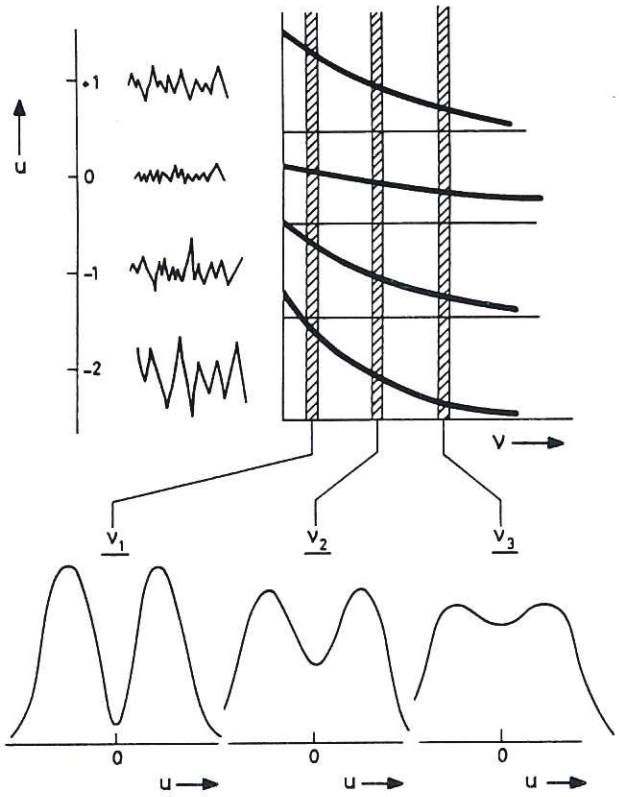

Fig.9 Schematic illustration of data analysis procedure. Fluctuations are recorded at a sequence of slit positions u. Each record is Fourier analysed to produce a power spectrum. Then the amplitude at fixed frequency ν is plotted as a function of u to generate fluctuation envelope profiles.

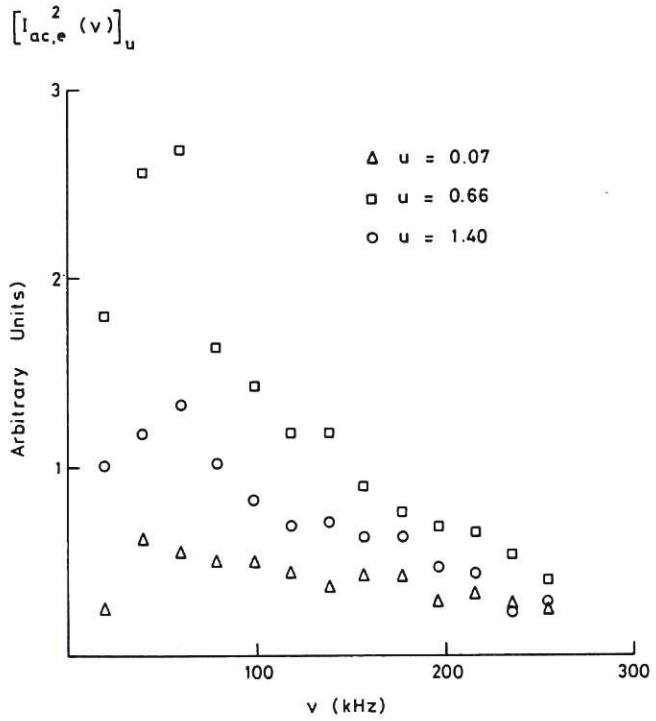

Fig.10 Power spectra of fluctuations at three slit positions, showing slit position dependence.

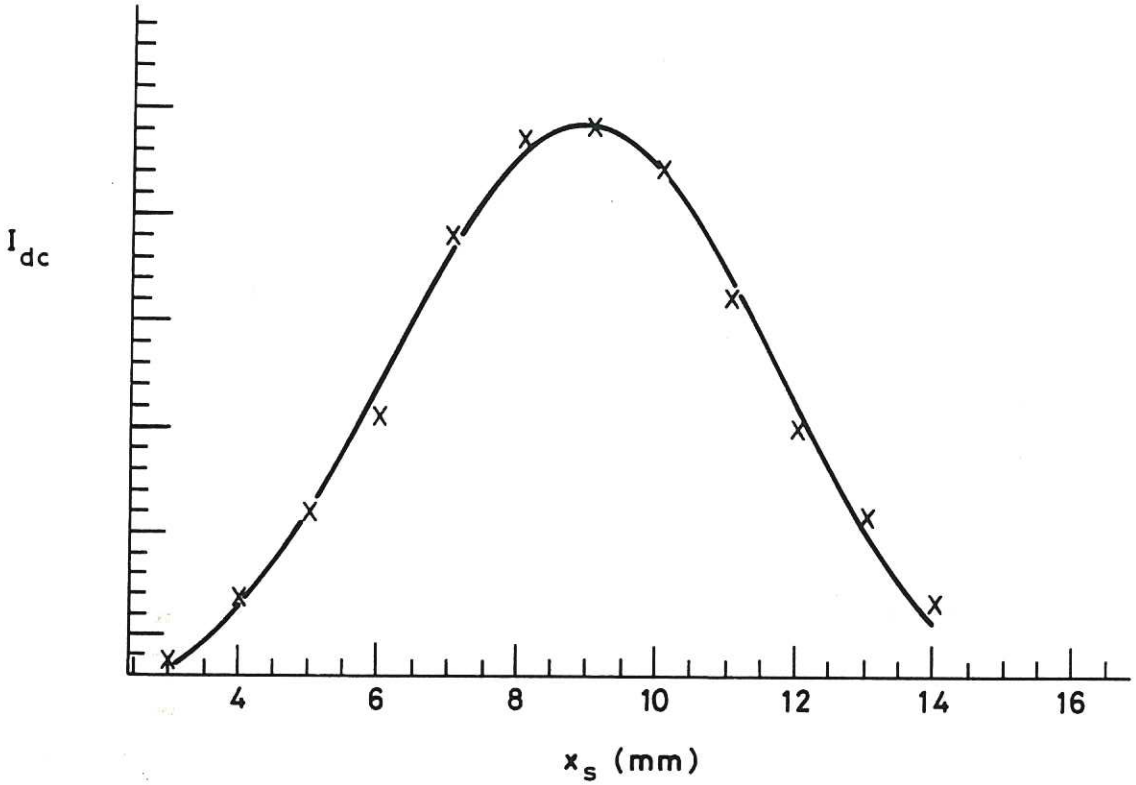

Fig.11 Time independent profile I_{dc} of laser beam at the slit plane, and the best-fit gaussian through measured points.

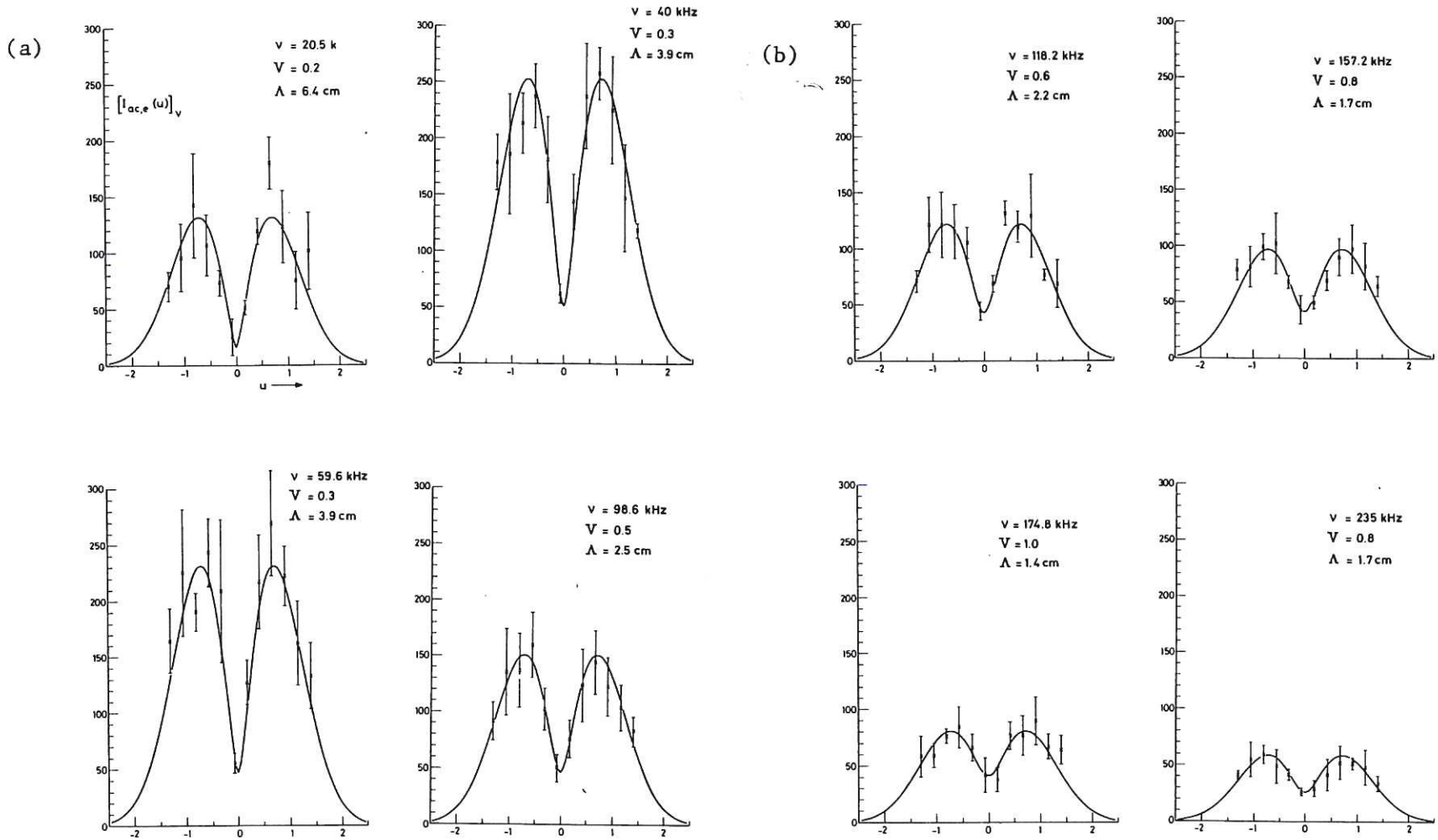

Fig.12 Examples of measured time-dependent beam profile envelopes for the first ms of the reproducible plasmas investigated. Each profile corresponds to a discrete frequency ν. Best fit theoretical curves characterized by the parameter V, from which wavelength Λ is deduced, are illustrated.

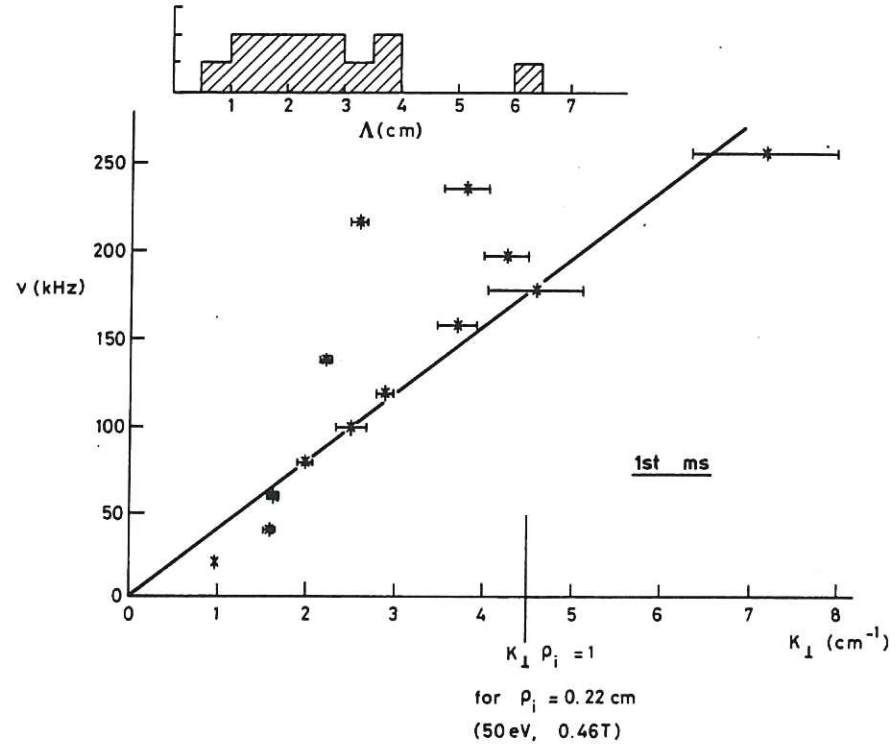

Fig.13 Frequency plotted against wavenumber $\kappa_\perp$ (cm^{-1}) for fluctuations during the first ms. The value of $\kappa_\perp$ for which $\kappa_\perp \rho_i = 1$ for prevailing plasma conditions is shown. Inset is histogram of corresponding wavelengths.

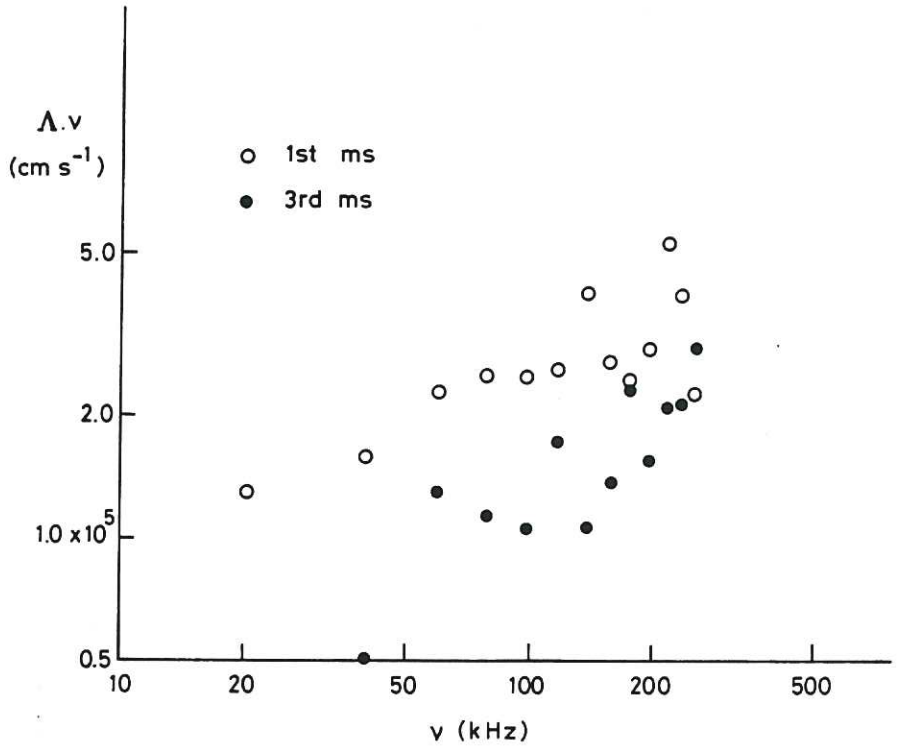

Fig.14 Phase velocities $\Lambda \cdot \nu$ for the first and third ms intervals.

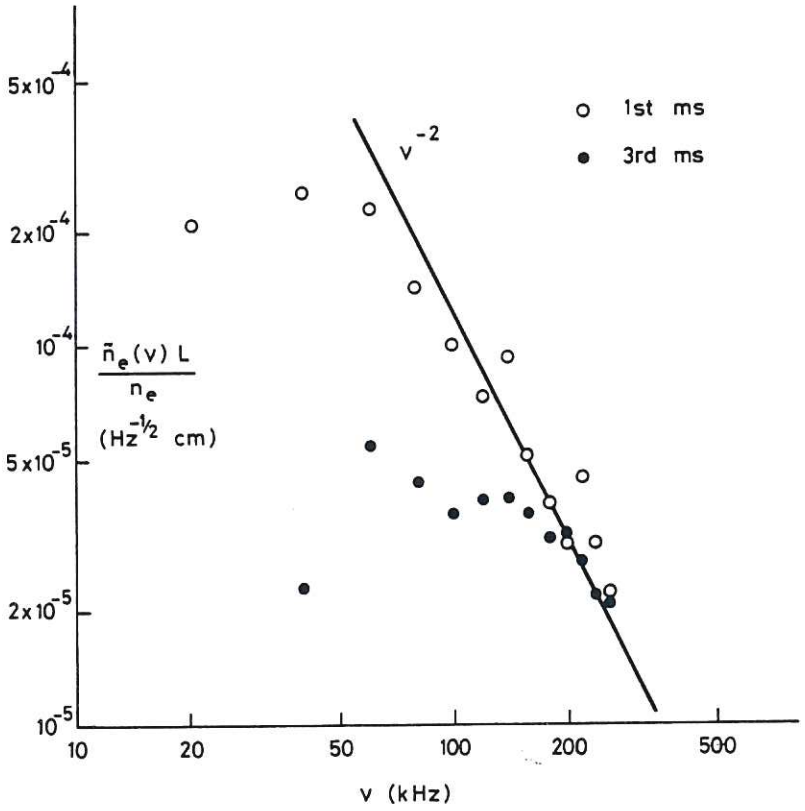

Fig.15 Frequency spectra of fluctuations for the first and third ms intervals deduced via envelope curve fitting process described in the text.

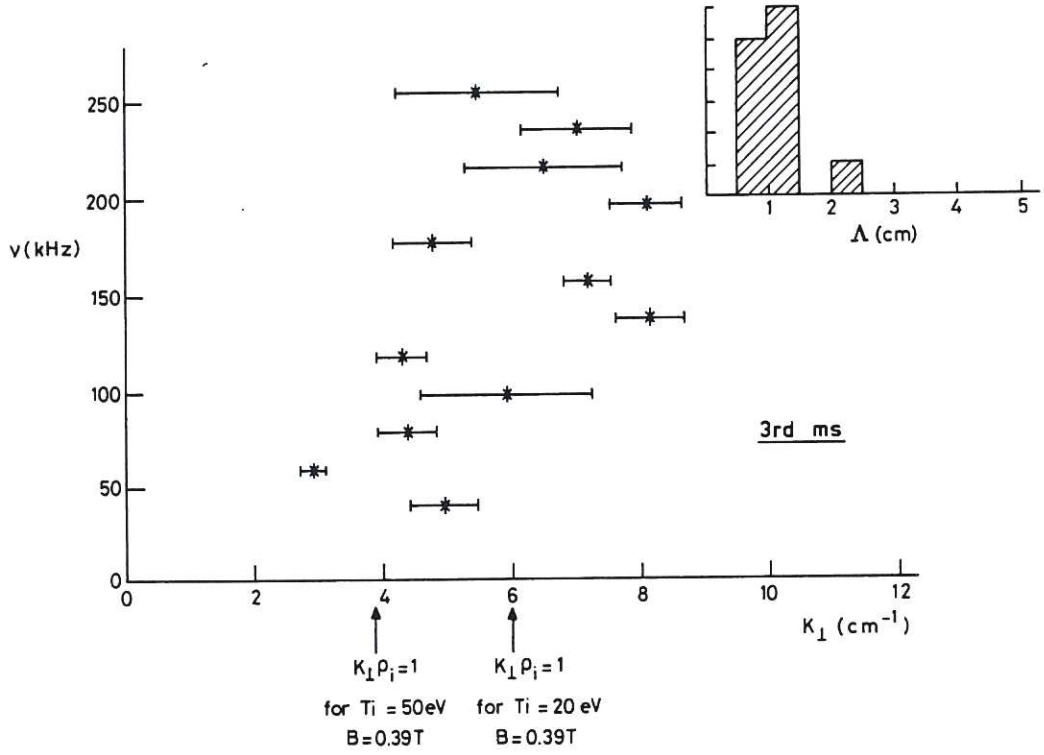

Fig.16 Frequency versus wavenumber $\kappa_\perp$ for fluctuations during third ms interval. Inset shows wavelengths to be clustered around $\Lambda \sim 1$ cm in contrast to the first ms interval.

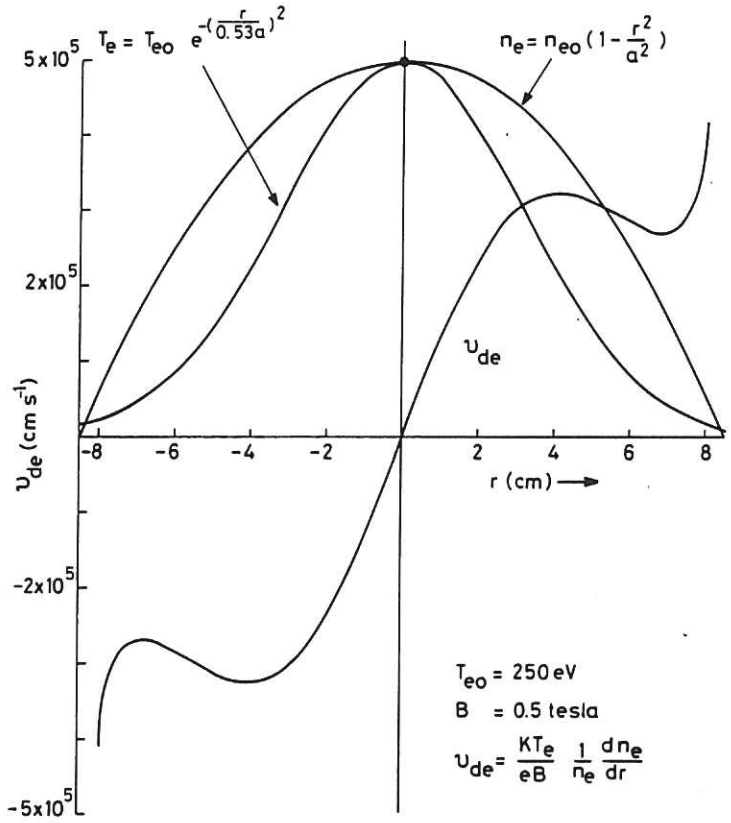

Fig.17 Electron magnetic drift velocity across TOSCA plasma profile calculated from density and electron temperature profiles. Drift velocities in the "transport" region, 1–7 cm, agree well with measured wave phase velocities.

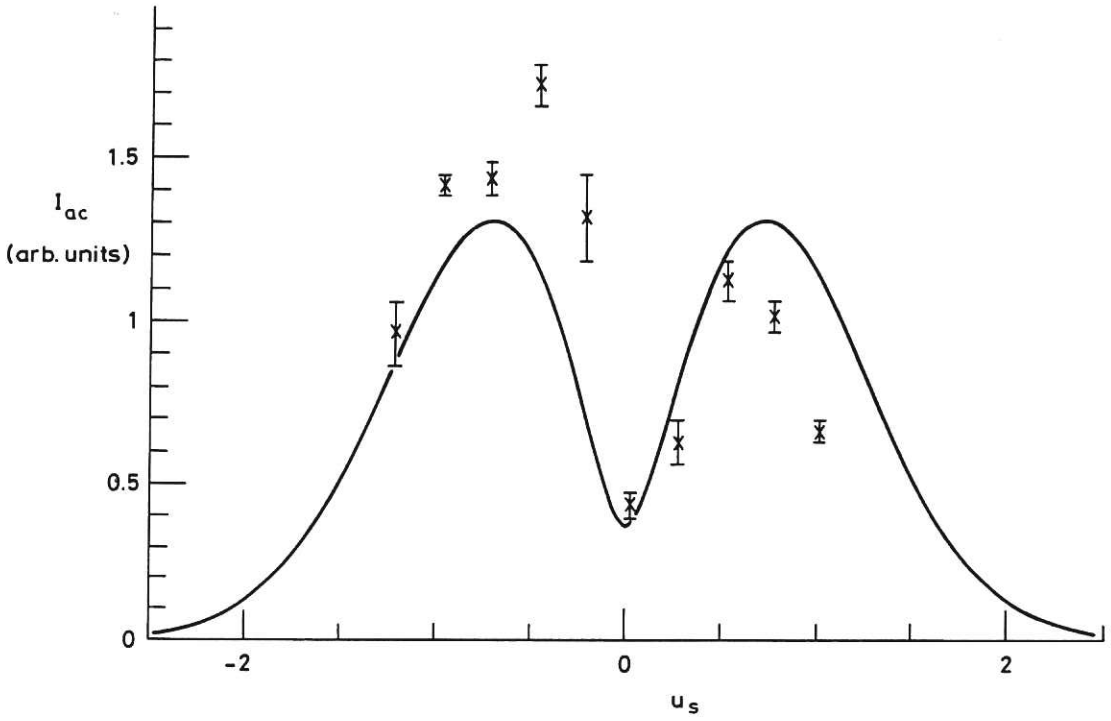

Fig.18 An asymmetric beam profile, illustrating its marked departure from "best fit" theory.